Retrieval of at-sensor irradiance using Incident Light Sensor (*ILS*)[*]

Kyu-Young Choi and Edward J. Milton
Department of Geography, University of Southampton,
Southampton SO17 1BJ, Hampshire, UK

ABSTRACT

A number of aircraft sensors have the facility to measure spectral downwelling irradiance using a sensor mounted on the roof of the aircraft, but these data are rarely used for atmospheric correction. Part of the problem is that the attitude of the airborne platform is always changing during flight, even in stable conditions, so that direct use of data from an incident light sensor (ILS) can introduce errors into atmospheric correction methods.

The continual motion of the ILS is used here to advantage, as a means to fit a sky radiance distribution model developed by Brunger and Hooper (1993) to data from the Itres Instruments CASI ILS. The inclination of the ILS sensor, due to changing aircraft attitude, is considered as the slope plane in the model. The selected model coefficients correspond to parameterised atmospheric conditions, i.e. clearness index and diffuse ratio. The ILS data corrected by the model are well-matched to variations of irradiance measured at ground level during three flights. The radiance distribution at sensor level is also calculated by the model, and shows the characteristics of the sky conditions at the time of each flight.

1.0 Introduction

The calibration of remotely sensed data is becoming increasingly important, as the applications of the remote sensing (RS) require more accurate information. In addition to the basic radiometric calibration, atmospheric correction is often essential for multi-temporal RS applications, for those focusing on dark targets, or for those in which physically meaningful units (e.g. spectral radiance, reflectance or albedo) are required. Incomplete or inaccurate atmospheric correction often results in failure of the most common uses of image data, such as mapping land-cover and land-cover change (Song *et al*., 2001).

Atmospheric correction of RS data from spaceborne sensors has been relatively well understood for many years, since it is simpler than that of airborne data. The relatively small field of view due to high altitude means less directional effects in reflected radiance from the ground, and more importantly, the radiance travels twice the complete thickness of the atmosphere between sensor and the ground target, and the solar irradiance at the top of the atmosphere is known. In airborne sensing, flying in the middle of the atmosphere, estimating atmospheric conditions is much more complicated than for spaceborne RS data. The altitude and direction of the flight are not always the same, indicating changes in the sun-target-sensor geometry (Wilson, 1995). These result in variations in incident illumination and in the amount of atmospheric scattering above the sensor level (Stokkom and Guzzi, 1984).

The feasibility of using an airframe-mounted spectrometer to measure spectral irradiance at aircraft altitude was investigated by Milton *et al*. (1994) using a Spectron Engineering SE-590 spectroradiometer. Two identical instruments, one with a cosine-corrected receptor for downwelling irradiance and the other with a nominal 1° field-of-view for upwelling radiance, were mounted outside of a Bell Jet Ranger helicopter. Multi-height measurements over uniform targets showed residual atmospheric effects in the reflectance spectra measured, which varied

[*] Presented at the Fifth International Airborne Remote Sensing Conference, San Francisco, California, 17-20 September 2001.

depending upon the thickness of atmosphere beneath the platform. The systematic nature of these variations suggested that an airframe-mounted irradiance sensor would be a useful addition to an aircraft sensor for atmospheric correction purposes, allowing the calculation of at-sensor reflectance and the temporal and spatial variability of the incident irradiance (Gray *et al*., 1997). However, the apparent usefulness of a rooftop probe is seriously compromised in data acquisition from fixed-wing platforms due to variations in downwelling irradiance signals caused by pitch, roll, and yaw of the platform.

Shepherd *et al* (1995) have analysed the errors involved in using data from a rooftop-mounted incident irradiance sensor fitted to the Itres Instruments Compact Airborne Spectrographic Imager (CASI) to calculate the reflectance of ground targets. Piekutowski *et al*. (1996) attempted to correct for variation in aircraft attitude on data from an incident light sensor fitted to the MEIS-II (Multispectral Electro-optical Imaging Scanner) (Piekutowski, *et al*., 1996). However, their attitude correction still needs the 5S radiative transfer model to estimate the ratio of direct to diffuse irradiance at altitude.

2.0 SLOPE IRRADIANCE MODEL

In practice, the aircraft attitude is always tilting toward a certain direction during the flight. As a cosine diffuser is mounted parallel to the body of the plane, the slope of the probe corresponds to the aircraft attitude. The irradiance on the cosine diffuser inclined toward the sun is greater than that on the horizontal plane, and vice versa.

There have been a number of empirical and analytical studies of irradiance on slopes (e.g. Brunger and Hooper, 1993; Gates, 1980), often developed for estimating the efficiency of solar panels to be used inclined on the top of buildings (Hooper and Brunger, 1980). The diffuse irradiance on the inclined surface is obtained by integrating the sky radiance distribution model over the sky dome visible to the surface with the horizontal global and diffuse irradiance measurements.

The simplest slope irradiance model is basically assumed that the distribution of the diffuse sky radiation is uniformly distributed over the dome. The isotropic model is only a function of slope angle,

$$G_{d,i} = G_d \left(1 + \cos(\alpha)\right)/2 . \quad \textbf{(1)}$$

It normally underestimates the diffuse irradiance from the clear sky conditions and approximates prediction of complete overcast. On the contrary, the diffuse irradiance coming from the direction of the sun is a heliocentric model that is a function of angular distance from the sun to a point of the sky,

$$G_{d,i} = G_d \left(\cos(\alpha) + \sin(\alpha)\cos(\phi)\tan(\theta)\right). \quad \textbf{(2)}$$

The model greatly overestimates the diffuse radiation as the slope inclines toward the sun. These two models represent the extreme sky conditions and rather unrealistic. Many authors develop the models predicting various sky conditions (for example, Hooper and Brunger, 1980 & 1987 as radiance model; Perez, 1993a & 1993b as luminance model). The performance of these different model were compared by Vartiainen (2000), and Perez's model (Perez, 1993a & 1993b) turned out to have the lowest error range amongst five sky irradiance and six sky radiance distribution models on slope. Brunger and Hooper's model (1993) is used in this study as it is one of the few sky radiance distribution models that cover the complete range of atmospheric conditions.

Although there is evidence indicating that radiance (unit W/m^2sr) and luminance (unit $lumen/m^2sr$) distributions are qualitatively similar, the radiance distribution model is more sensible for RS applications. Another important feature of the model is that it is a function of two parameterised atmospheric conditions, the clearness index (k_t) and diffuse fraction (k).

The model is based on Three-Component Continuous Distribution (TCCD) model (Hooper and Brunger, 1980), i.e. circumsolar (a_0), horizontal brightening (a_1), and a uniform background terms (a_2). And an extra coefficient (a_3) is set as a linear term. The model calibration was undertaken by finding the parameters. A number of field

experiments under a wide variety of atmospheric condition were sorted into bins defined by specific ranges of k_t and k. A set of measurements in each bin is statistically analysed for the model parameters.

Once the atmospheric condition is selected, its corresponding parameters are used to get the radiance (W/m^2sr) of the sky in the position of the dome (θ, ϕ),

$$L(\theta,\phi,\theta_s,\phi_s) = G_d\left[\frac{a_0 + a_1\cos\theta + a_2\exp(-a_3\Psi(\theta,\phi,\theta_s,\phi_s))}{\pi(a_0 + 2a_1/3) + 2a_2 I(\theta_s,a_3)}\right].^{\ddagger} \quad \textbf{(3)}$$

The distribution of radiance over the dome on a slope is used to calculate the ratio of sky irradiance on the slope to that which would be found on a horizontal surface, and to integrate the radiance over the sky dome visible to the surface.

$$G_{d,i} = G_d\frac{\int_{-\pi}^{\pi}\int_{\alpha_0}^{\pi/2} L(\theta,\phi,\theta_s,\phi_s)\cos\theta(\sin\theta\cos\alpha + \cos\theta\sin\alpha\cos\phi)\cdot d\phi d\theta}{\int_{-\pi}^{\pi}\int_{0}^{\pi/2} L(\theta,\phi,\theta_s,\phi_s)\cos\theta\sin\theta\cdot d\phi d\theta} \quad \textbf{(4)}$$

Depending on whether the position of the point on the dome is below horizon or not, the limit of inner integration is given by,

$$\alpha_0 = \begin{cases} 0 & \text{Where } -\pi/2 \le \phi \le \pi/2 \\ \arctan(-\tan\alpha\cos\phi) & \text{Otherwise} \quad 0 \end{cases}$$

3.0 DATA DESCRIPTION

On 3 September 1999 the intertidal vegetation bordering the West Solent, Hampshire, UK, was surveyed using CASI from the Environment Agency (EA) on behalf of English Nature. Over 30 flightlines were flown at an altitude of 2,500 feet between 09:00 and 12:40. The CASI was configured in spatial mode using the intertidal bandset recommended by Thomson *et al*. (1998).

Image	Time (GMT)	Heading (Degree from the North)	Solar Azimuth (Degree from the North)	Relative sun angle (= heading–solar azimuth)
Imag4315	9:20:16 to 9:21:35	232	126	106
Imag4332	10:40:16 to 10:41:56	55	150	-95
Imag4354	12:36:20 to 12:37:37	231 (331)	191	40

Table 1. Flight information overpass of the calibration site. Figures in brackets indicate information in *.inf file, which are suspected as being in error, based on the map provided and the image orientation.

During the period of the aerial survey, three flight lines passed over the Beaulieu Heath Calibration Site (BHCS; approximately N50.40°, W1.23°) where a Spectron SE-590 spectroradiometer was located and continuously

---

‡ Where

$$I(\theta_s,a_3) = \frac{[1+\exp(-a_3\pi/2)]}{(a_3^2+4)}\cdot \left\{\pi - \left[1 - \frac{2[1-\exp(-a_3\pi)]}{\pi a_3[1+\exp(-a_3\pi/2)]}\right]\cdot[2\theta_s\sin\theta_2 - 0.02\pi\sin(2\theta_s)]\right\} \quad \textbf{(5)}$$

and the angular distance in radians between (θ, ϕ) and (θ_s, ϕ_s),

$$\Psi(\theta,\phi,\theta_s,\phi_s) = \arccos[\sin\theta\sin\theta_s\cos(\phi-\phi_s) + \cos\theta\cos\theta_s] \quad \textbf{(6)}$$

measuring downwelling irradiance over the spectral range from 368 to 1114 *nm*. The data from the SE-590 were integrated over the spectral range and plotted for the series of measurements (Figure 1). The solar flux reaching the ground is modelled by using the 6S code and superimposed upon the ground measurements. The difference between them (grey region in Figure 1) slightly increases with time. Between around 09:00 and 10:45 the solar irradiance steadily increased as the early morning mist cleared, and there was an interval during which the solar irradiance changed rapidly as high level cloud passed over the area. Soon after such disturbances, the irradiance became stable, and remained so until the end of the survey.

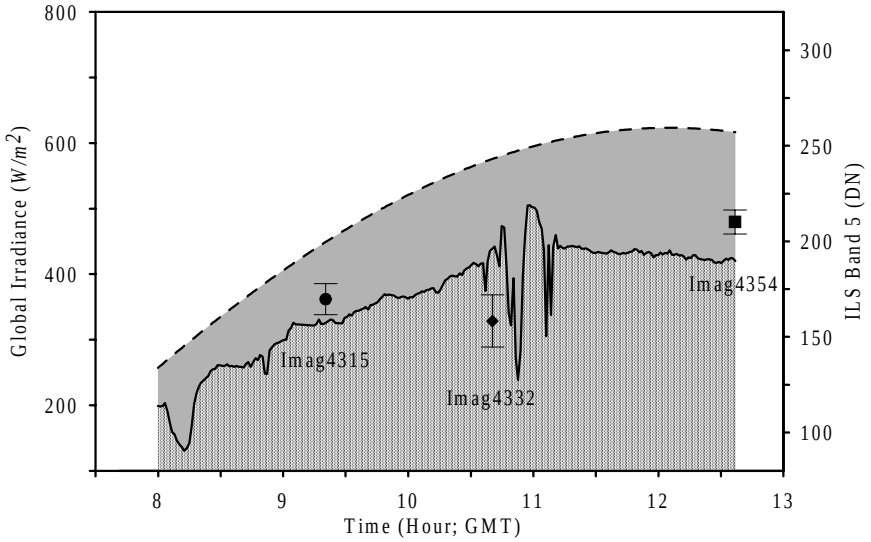

Figure 1. Global irradiance at ground in Beaulieu Heath calibration site (solid line), and the solar flux modelled by 6S (dotted line). The grey area represents the difference between those two. The mean DN values of the ILS from three flights over the calibration site are superimposed with their standard deviation ranges.

In the CASI system, the incident light sensor (ILS) is a cosine-corrected receptor fitted horizontally in the roof of the aircraft (Figure 2). The sensor head is connected to the CASI via an optical fibre. Light from the ILS is imaged onto the hidden section of a two-dimensional CCD array, and recorded in spectral bands identical to those from the scene viewed by the CASI. As the CASI was configured in spatial mode, the ILS data are recorded in column of 512 in each line of image data. No calibration of ILS data to irradiance units was available for this particular sensor. The data from the ILS are strongly affected by the direction of flight relative to the sun, i.e. a mean ILS of Imag4332, a flightline away from the sun, is lower than irradiance at ground whereas the others are greater as the flightline is heading relatively toward the sun

Figure 2. A picture of ILS quoted from ITRES™ world wide web (http://www.itres.com).

Since a cosine receptor mounted on an aircraft is sensitive to the inclination of the sensor in relation to the sun, it is necessary to take account the deviation of the aircraft from level flight. Attitude parameters of pitch and roll were recorded in DN for every line of the image, and converted to angles in degrees by post-processing. A positive pitch indicated the nose of the aircraft rising above the horizon, and vice versa. A positive roll represented the port wing dropping below the horizon. Yaw was not recorded for the particular CASI installation we used. Plots of pitch and roll recorded during the flights show that pitch is positive at around 20° depending on the speed of the plane, while roll values fluctuate throughout the flightline.

4.0 RESULTS

Brunger and Hooper's model (1993) described above is applied to the ILS data. The model is originally developed in order to find irradiance on slope ($G_{d,i}$) from known atmospheric conditions (k_t, k). In the case of the ILS data, on the other hand, objective is to calculate irradiance in horizontal level as if the ILS lies on a horizontal plane at sensor altitude, as well as atmospheric conditions.

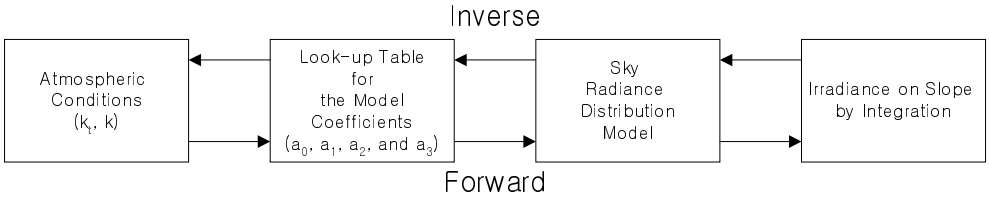

Figure 3. Schematic diagram of sequence of Brunger and Hooper's model.

The sequence of numerical calculation of the model therefore follows inversely, though it is not a true inverse (Figure 3). A table of the model coefficients obtained by intensive field experiments over a wide variety of atmospheric conditions was used as input data. A total of 48 sets of model coefficients over specific ranges of k_t and k are applied to the model with solar positions (θ_s, ϕ_s), slope angle (α), and its direction relative to the sun.

The aircraft attitude data had to be pre-processed before applying the model. To find the accurate degree of slope and its direction is significant as the model is sensitive to the inclined surface in relation to the sun position. The aircraft attitude is expressed by pitch and roll with respect to the flight direction. Although pitch is greater than roll (see Figure 5a) so that flight direction may be considered as fixed slope direction during the flight, line-by-line calculations using pitch and roll result variations of more than ±10° in slope direction and ±5° in slope angle. Such variations in slope causes equivalent differences in sun position.

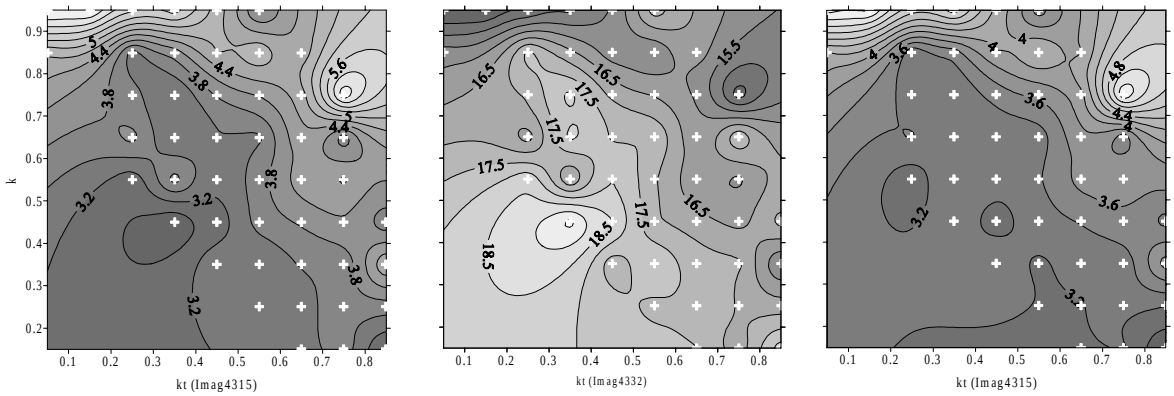

Figure 4. RMS contour plots over the look-up table of atmospheric condition (k_t k). White crosses represent the points of available model coefficients (Brunger and Hooper, 1993).

Since each flightline took less than 2 minutes over a linear distance of less than 10 km, it is assumed that atmospheric condition above at-sensor level is relatively uniform and invariable. Therefore, the irradiance on the horizontal surface calculated from the model is assumed to be uniform as well. The uniformity of the irradiance over line number of each image data was found using the Root Mean Square (RMS) deviation as a convenient measure of the spread around the mean. The lowest region in the look-up table represented the most appropriate for the ILS correction. The contour plots of RMS in each flightline show that the position of the lowest RMS region varied, indicating atmospheric conditions changed during the survey. In comparison with the field measurements during the flights (Figure 1), Imag4315 was affected by the early morning mist and results show relatively low atmospheric clearness index (k_t = 0.35) with moderate diffuse ratio (k = 0.45). Imag4332 was collected just before the high level cloud (k = 0.75), while steady increases of irradiance was about to settle (k_t = 0.75). In the last flight (Imag4354), atmospheric condition above altitude of the flight became clear and stable. Atmospheric clearness index (k_t = 0.85) was similar to the previous flight (Imag4332) – the amount of irradiance at ground in both flights was similar, though it was more unstable in Imag4332 –, but diffuse irradiance with respect to the global irradiance was reduced (k = 0.15).

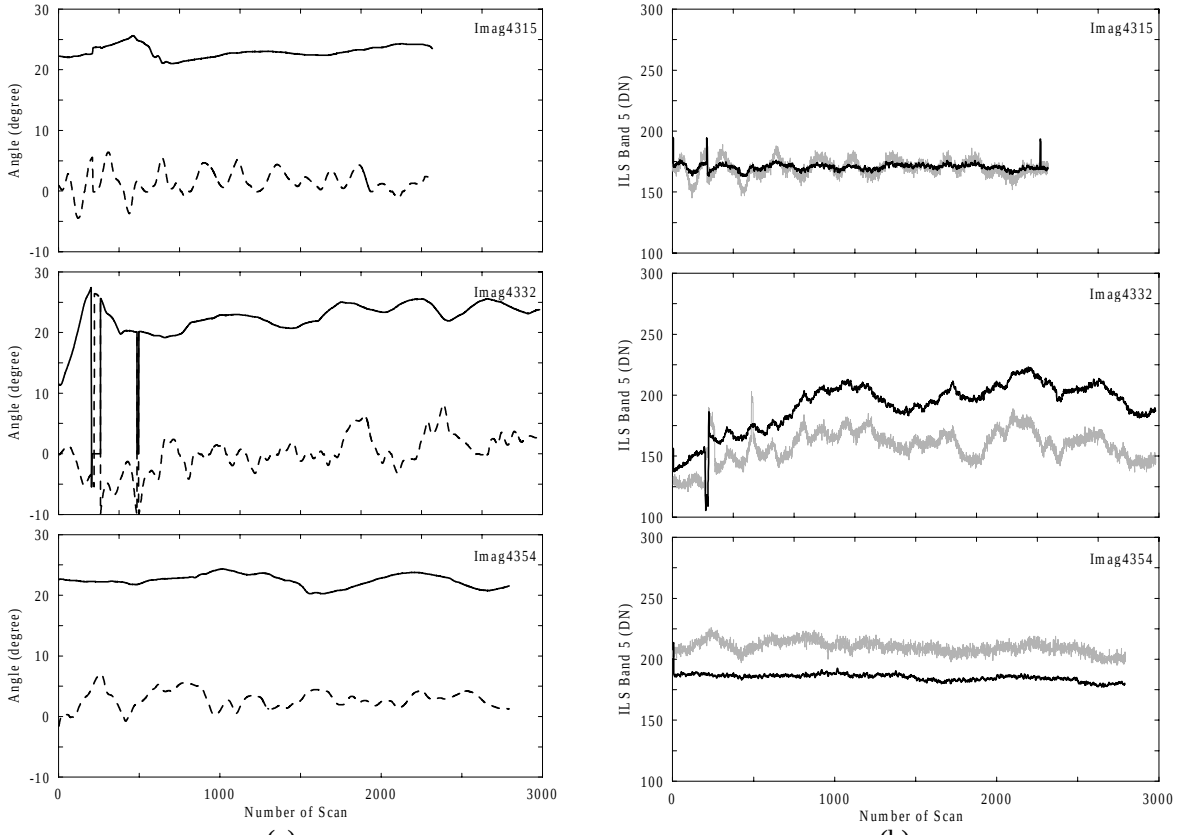

Figure 5. Plots of pitch (solid line) and roll (dotted line) in each flight (a). In (b), 7-scan-averaged raw ILS (grey) is superimposed on the model corrected ILS plot (black).

The model coefficients determined in each flight from the parameterised atmospheric conditions above were used for the irradiance on a horizontal surface at sensor level (Figure 5b). In order to reduce the high frequency errors, the ILS data were averaged over 7 scans. The effects of plane attitude on the ILS data are effectively minimised, and the corrected ILS decrease in Imag4315 and Imag4354 while increase in Imag4332. Mean values after correction follow the trend of irradiance changes at ground quite well (see Figure 1). The variations, still shown after the correction, may be due to internal ILS error or actual atmospheric variations over the flight region. The

ILS correction on Imag4332 is rather poorer than the others. It may be thought of unstable atmospheric conditions during the flight. However, incorrect information on flight direction possibly caused the problem (E.M. Rollin, personal communication), since corrected ILS still tends to have similar trend of original ILS data.

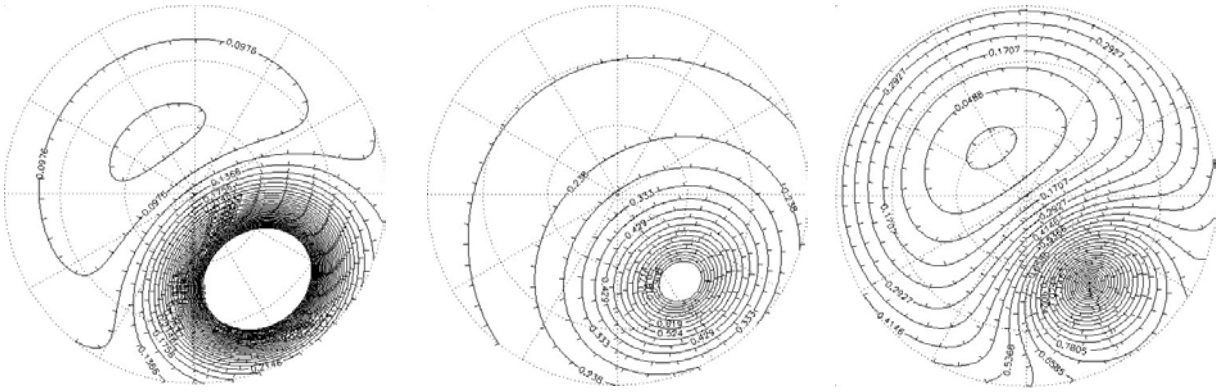

(a) (b) (c)

Figure 6. Stereonet representation of the sky radiance distribution for each of the three flights (Imag4315 (a), Imag4332 (b), and Imag4354 (c)), calculated using the Brunger and Hooper model.

In addition to atmospheric characteristics and ILS correction from aircaft attitude, at-sensor sky radiance distributions were given by the model calculations (Figure 6). The radiance of the sky was calculated by using Equation 3. Stereonet plots of the sky distrbution during the acquisition of Imag4315 and Image4354 show a similar pattern whereas that from Imag4332 looks close to the radiance distribution under a cloudy sky. On the other hand, the magnitudes of the radiance are similar in Imag4332 and Imag4354, both being much larger than Imag4315 which has radiance more concentrated in the sun's direction.

5.0 CONCLUSION

A sky radiance distribution model developed by Brunger and Hooper (1993) has been applied to CASI Incident Light Sensor data in order to estimate the downwelling solar irradiance at the aircraft. Continuous slope changes of the ILS sensor due to variations of the aircraft attitude is a problem in the direct use of the ILS data, but this helps in finding optimum coefficients for the model. The model results a unique set of coefficients for each flightline, which relates to the parameterised atmospheric condition. Radiance distributions at sensor level for different flightlines characterise different atmospheric conditions. Distributions of radiance depend upon the sun position and atmospheric turbidity but the angular distribution remains generally characteristic of single scattering (Shepherd and Xu, 1993).

GLOSSARY

a_0, a_1, a_2, a_3	Parameters of assignable value that allow the sky radiance model to respond to the atmospheric radiation conditions
G_d	Horizontal diffuse radiance
$G_{d,I}$	Diffuse radiance on inclined surface
G_h	Global solar irradiance on a horizontal surface
k	Diffuse fraction, G_d/G_h. A ratio of the diffuse irradiance on a horizontal surface to the global irradiance on a horizontal surface. Ranges from 0 to 1
k_t	Atmospheric clearness index G_h divided by the local extraterrestrial solar irradiance on a horizontal surface; the extraterrestrial solar irradiance is a deterministic function of date, time, and the local latitude. Ranges from 0 to 1.
L	Sky radiance

θ	Angular distance from the zenith in radians
ϕ	Angle measured in radians clockwise in the horizontal plane from the North
(θ_s,ϕ_s)	Coordinate of the direction of the sun
Ψ	Angular distance in radians between the direction of the solar disk and the direction (θ,ϕ)
α	Slope of the plane

ACKNOWLEDGEMENT

The authors gratefully acknowledged the provision of CASI and aircraft attitude data from the UK Environmental Agency. Jennifer Youngberg, University of Waterloo, Canada, kindly provided an original source code of the model. Kyu-Young Choi is grateful for funding from the University of Southampton High Performance Computing Initiative. The UK Natural Environment Research Council Equipment Pool for Field Spectroscopy supported this work through advice from Dr Elizabeth Rollin and by the loan of a field spectroradiometer.

REFERENCES

Brunger, A. P., Hooper, F. C., 1993, *Anisotropic sky radiance model based on narrow field of view measurements of shortwave radiance*, Solar Energy, 51, 1, 53-64, Erratum: 51, 6, 523p.

Gary, L., Freemantle, J., Shepherd, P., Miller, J., Harron, J., Hersom, C., 1997, *Characterization and Calibration of the CASI airborne imaging spectrometer for BOREAS*, Canadian Journal of Remote Sensing, 23, 2, 188-195p.

Gates, D.M., 1980, Biophysical Ecology, Springer-Verlag, New York, 611p.

Hooper, F. C., Brunger, A. P., 1980, *A model for the angular distribution of sky radiance*, *Journal of Solar Energy Engineering*, 102, 196-202p.

Hooper, F. C., Brunger, A. P., Chan, C. S., 1987, *A clear sky model of diffuse sky radiance*, Journal of Solar Energy Engineering, 109, 9-14p.

Milton, E.J., Blackburn, G.A., Rolling, E.M., Danson, F.M., 1994, *Measurement of the spectral directional reflectance of forest canopies: a review of methods, and a practical application*, Remote Sensing Review, 10, 285-308.

Perez, R., Seals, R., Michalsky, J., 1993a, *All-weather model for sky luminance distribution – Preliminary configuration and validation*, Solar Energy, 50, 235-245.

Perez, R., Seals, R., Michalsky, J., 1993b, *Erratum to All-weather model for sky luminance distribution – Preliminary configuration and validation*, Solar Energy, 51, 423.

Shepherd, P.R., O'Neil, N.T., Piekutowski, T., 1995, *Analysis of downwelling and upwelling diffuser probe data to determine at-sensor irradiance fluxes*, Proceedings of the 17th Canadian Symposium on Remote Sensing, Canadian Remote Sensing Society, Saskatoon, Saskatchewan, June 13-15, 337-342.

Shepherd, P.R., Xu, Q. F., 1993, *An error analysis of a reflectance conversion methodology using an irradiance sensor*, Proceedings of 16th Canadian Symposium on Remote Sensing, 841-845p.

Song, C., Woodcock, C.E., Seto, K.C., Lenney, M.P., Macomber, S.A., 2001, *Classification and change detection using Landsat TM data: When and how to correct atmospheric effects?*, Remote Sensing of Environment, 75, 230-244.

Stokkom, H,T.C. van, Guzzi, R., 1984, *Atmospheric spectral attenuation of airborne remote-sensing data comparison between experimental and theoretical approach*, International Journal of Remote Sensing, 5, 6, 925-938.

Thomson, A.G., Fuller, R.M., Sparks, T.H., Yates, M.G., Eastwood, J.A., 1998, *Ground and airborne radiometry over intertidal surfaces: Waveband selection for cover classification*, International Journal of Remote Sensing, 19, 1189-1205.

Vartiainen, E., 2000, *A new approach to estimating the diffuse irradiance on inclined surface*, Renewable Energy, 20, 45-64p.

Wilson, A.K., 1995, *NERC scientific services airborne remote sensing facility user guide handbook*, Natural Environment Research Council, 72p.